SUPPLEMENTARY DATA

Supplementary Material and Methods

Materials. Starting materials, reagents, and solvents were purchased from Sigma-Aldrich (St. Louis, MO) or Alfa Aesar (Ward Hill, MA).

General Methods. ^{1}H- (400 MHz) and ^{13}C-NMR (100 MHz) spectra were acquired at room temperature with an Avance 400 instrument (Bruker; Billerica, MA) using the chemical shifts of residual deuterated solvents as internal standard. Chemical shifts (δ) are reported in ppm downfield relative to the signal for tetramethylsilane (TMS). The abbreviations d, dt, and m represent doublet, doublet of triplet, and multiplet, respectively. High resolution mass spectrometry (HRMS) images were acquired with electron spray ionization at the Mass Spectrometry Laboratory, University of Illinois at Urbana-Champaign (Urbana, IL). Liquid chromatography–mass spectrometry (LC-MS) spectra were acquired with an LCQ DECA instrument (Thermo Fisher Scientific; Waltham, MA) fitted with a Luna C18 column (5 μm; 2.0 × 150 mm; Phenomenex; Torrance, CA) eluted at 150 μL/min with MeOH-H_2O. Radioactivity measurements were corrected for physical decay.

2-((3-Fluoro-5-iodophenyl)ethynyl)pyridine (3). 2-Ethynylpyridine (124 mg, 1.2 mmol), 3,5-diiodofluorobenzene (490 mg, 1.4 mmol), CuI (15 mg, 79 μmol), *bis*(triphenylphosphine)palladium(II) dichloride (27 mg, 39 μmol), and triethylamine (0.5 mL) were added to 1,2-dimethoxyethane (5 mL). Argon was then bubbled into the solution while it was heated to 80°C. The resulting black reaction mixture was heated at 80°C until thin layer chromatography showed no starting material present (10-12 hours). The reaction mixture was then cooled to room temperature, filtered through celite, and evaporated to dryness. The residue was dissolved in ethyl acetate (25 mL) and washed with H_2O (20 mL × 2) and then brine (20 mL × 2). The organic phase was dried ($MgSO_4$) and evaporated under vacuum. The residue was purified by chromatography (silica gel; hexanes-AcOEt, 80: 20 v/v) to afford **3** (179 mg, 46%) as an off-white powder. mp: 106–108 ºC. ^{1}H-NMR ($CDCl_3$): δ 8.64 (dt, 1H, J_1=4.02 Hz, J_2=0.82 Hz,), 7.75 (t, 1H, J=1.20 Hz), 7.71 (dt, 1H, J_1=7.61 Hz, J_2=1.66 Hz), 7.53 (d, 1H, J=7.84 Hz), 7.45 (dt, 1H, J_1=7.00 Hz, J_2=1.50 Hz), 7.28 (m, 2H); ^{13}C-NMR ($CDCl_3$): δ 161.7 (d, J=252.35

Hz), 150.2, 142.6, 141.9, 136.5 (d, *J*=43.88 Hz), 127.4, 125.7 (d, *J*=15.84 Hz), 125.6, 123.4, 118.4 (d, *J*=22.92 Hz), 93.4 (d, *J*=8.94 Hz), 90.5, 85.8; HRMS: calculated for $C_{12}H_7F_2INS$ (M^+ + H), 323.9680; found, 323.9672; purity> 99.5% by radio high performance liquid chromatography (HPLC) on a Luna C18 column (10 μm, 4.6 mm × 250 mm) eluted with a mixture (45: 55 v/v) of MeCN-10mM $HCOONH_4$ at 3 mL/min, with eluate monitored for absorbance at 254 nm (t_R, 19.6 min).

Radiochemistry

Production of no carrier-added [^{11}C]hydrogen cyanide. No carrier-added (NCA) [^{11}C]carbon dioxide was produced from a PETtrace cyclotron (GE Medical Systems; Milwaukee, WI) with the $^{14}N(p,\alpha)^{11}C$ reaction by irradiating nitrogen gas (initial pressure 140 psi; volume, 80 mL) containing 1% oxygen with a proton beam (15.9 MeV, 45 μA) for 50 minutes. The [^{11}C]carbon dioxide (~ 55 GBq) was then trapped on a molecular sieve (13X, 80−100 mesh, 0.55 g) housed in a stainless steel column at 40^{o}C, while untrapped [^{13}N]nitrogen was directed to waste. The [^{11}C]carbon dioxide was released from the heated (350^{o}C) molecular sieve in nitrogen (250 mL/min), and then mixed with hydrogen (30 mL/min) and passed over heated (400^{o}C) nickel (Ni-3266, Engelhard Corp.; Iselin, NJ) housed in a quartz column (13 mm OD × 200 mm). The column effluent was passed through an oxygen scrubber (Oxisorb®; Sigma-Aldrich), mixed with anhydrous ammonia (20 mL/min; research grade; Matheson; Montgomeryville, PA) and passed over heated (950^{o}C) platinum wire (4.0 g, 0.2 mm OD × 20 mm; Sigma-Aldrich) housed in a quartz tube (9 mm OD × 200 mm). The effluent gas contained the NCA [^{11}C]hydrogen cyanide.

Supplementary Figures

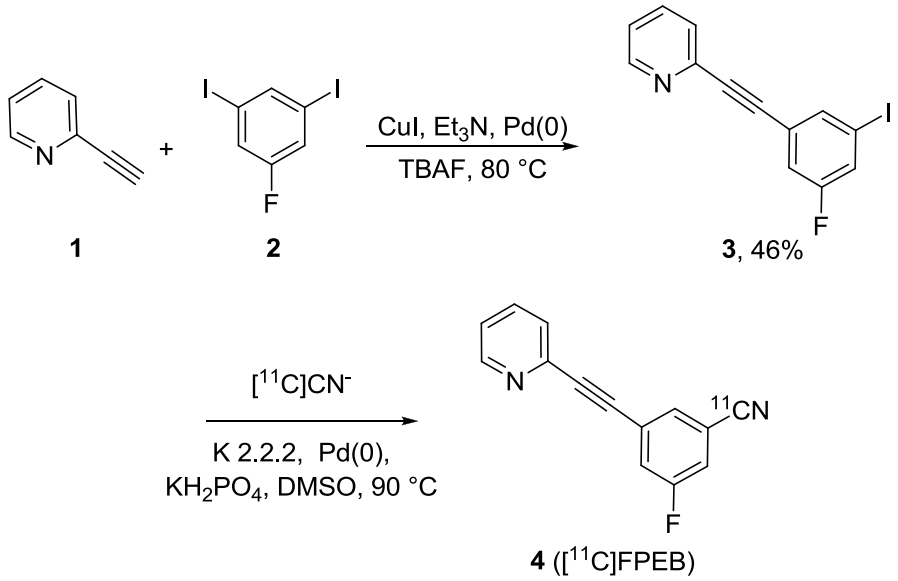

Supplementary Fig. 1. Synthesis of precursor **3**, and [^{11}C]FPEB (**4**).

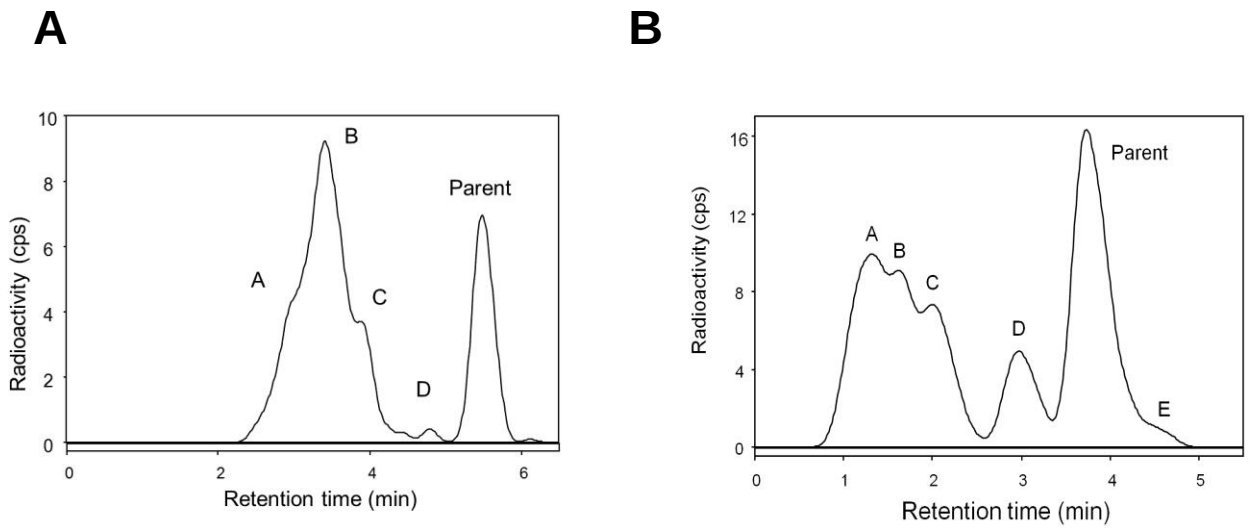

Supplementary Fig. 2. HPLC radiochromatograms illustrating plasma composition at 30 minutes after [^{11}C]FPEB injection **(A)** and at 40 minutes after [^{11}C]SP203 injection **(B)** in two different subjects. Radioactivity was measured in counts per second (cps).

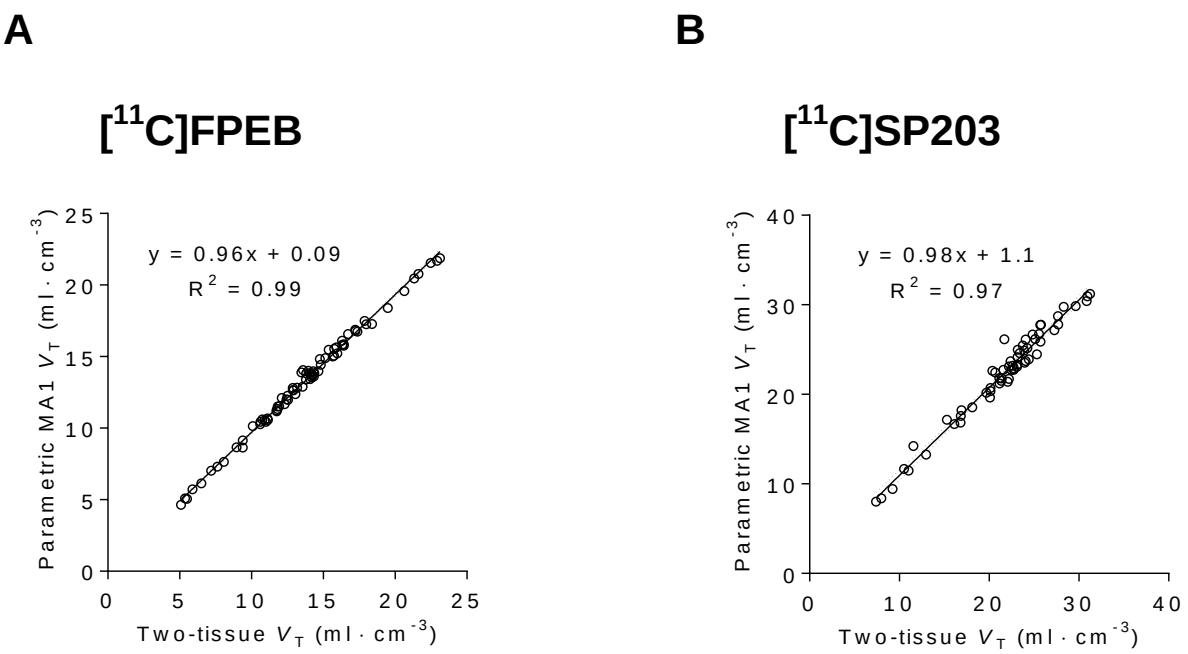

Supplementary Fig. 3. Scatter plot comparing V_T values by the $MA1_{voxel}$ method vs. two-tissue compartmental fitting from each of 10 brain regions from eight subjects for [^{11}C]FPEB (**A**) and six subjects for [^{11}C]SP203 (**B**). The simple linear regression was significant ($p<0.0001$), with a linear regression line equation and R^2 values as indicated on the plots. The solid line represents the line of best fit. Dashed lines are 95% confidence intervals.

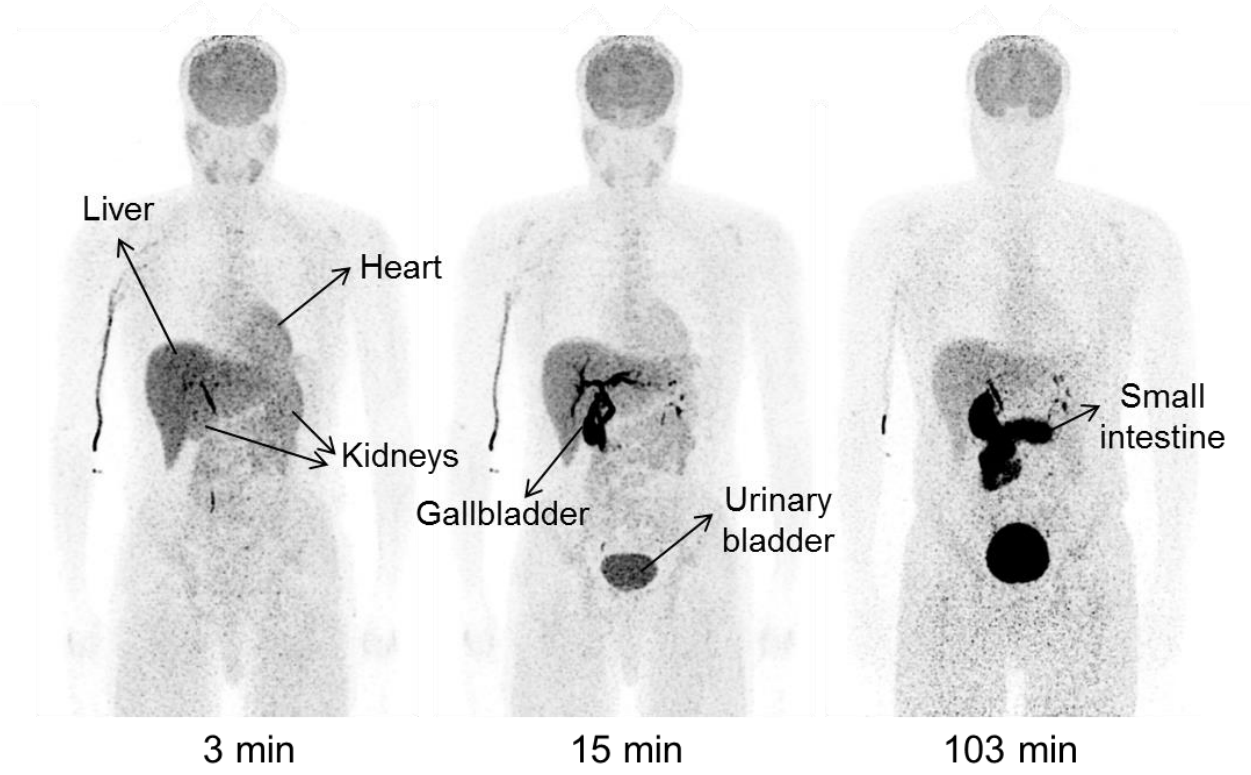

Supplementary Fig. 4. Whole-body maximum intensity projection (MIP) images of a healthy 26-year old male show the distribution of radioactivity at about 3, 15, and 103 minutes after injection of 352 MBq of [^{11}C]SP203. In addition to high uptake in brain, the image at three minutes shows high uptake in heart, liver, and kidneys, which have high blood perfusion. Images at 15 and 103 minutes show both hepatobiliary and urinary excretion of radioactivity and accumulation of activity in red marrow.

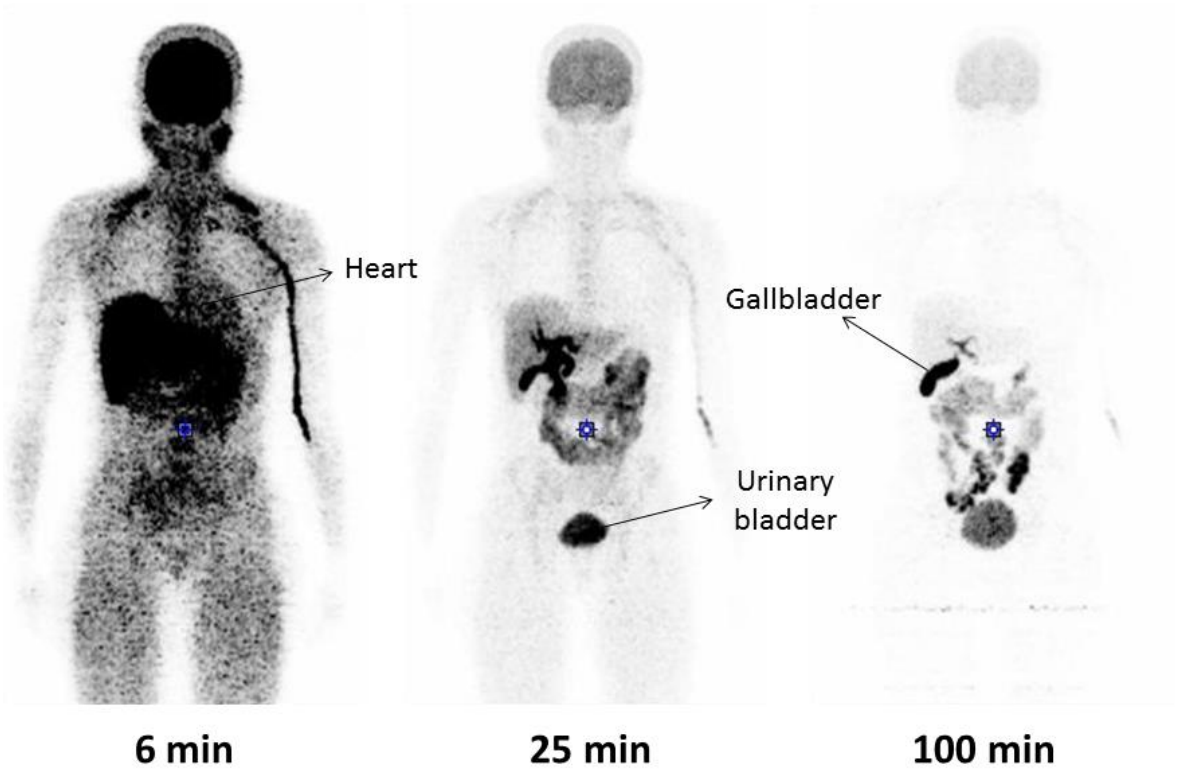

Supplementary Fig. 5. Whole-body maximum intensity projection (MIP) images of a healthy 33-year old female show the distribution of radioactivity at about 6, 25, and 100 minutes after injection of 364 MBq of [^{11}C]FPEB. In addition to high uptake in brain, the image at 25 minutes shows high uptake in heart, liver, and kidneys, which have high blood perfusion. Images at 25 and 100 minutes show both hepatobiliary and urinary excretion of radioactivity.

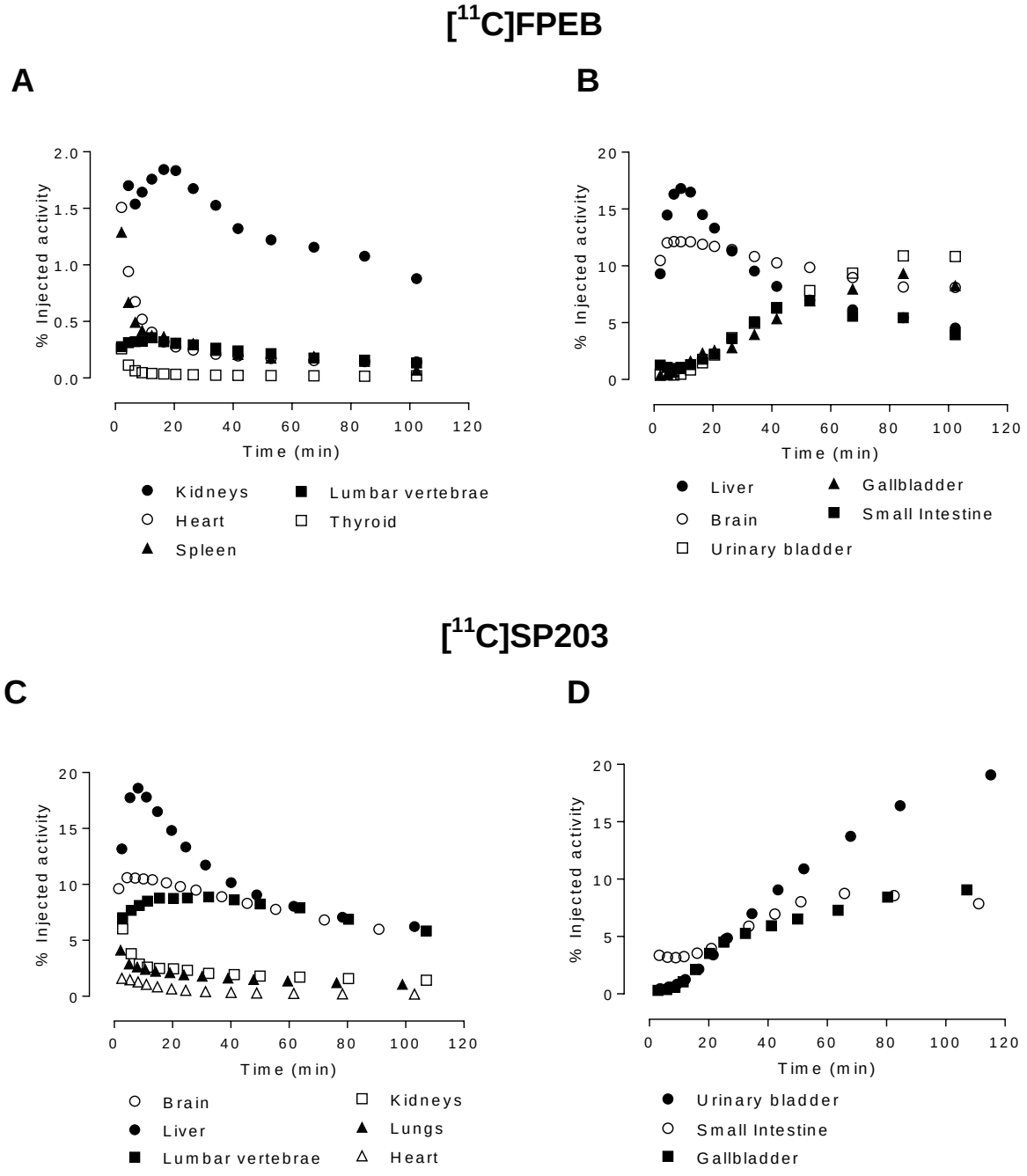

Supplementary Fig. 6. Time-activity curves for 10 source organs after [^{11}C]FPEB injection **(A and B)** and nine source organs after [^{11}C]SP203 injection **(C and D)**. Data are corrected for radioactive decay and expressed as mean from eight and six subjects for [^{11}C]FPEB and [^{11}C]SP203, respectively.

Supplementary Tables

Supplementary Table 1. Distribution volume (V_T) of [^{11}C]FPEB in human brain analyzed from large regions and individual voxels

	V_T (mL•cm^{-3})							
	Region					Voxel		
Brain regions	Two-comp	Logan $_{VOI}$		MA1$_{VOI}$		Logan $_{Voxel}$		MA1 $_{Voxel}$	
Temporal cortex	17.3	16.9	(-2.3%)	16.8	(-2.9%)	15.6	(-9.8%)	16.3	(-5.8%)
	± 3.0	± 2.6		± 2.6		± 4.5		± 4.5	
Cingulate	15.9	15.7	(-1.3%)	15.6	(-1.9%)	14.5	(-8.8%)	15.1	(-5%)
	± 3.2	± 2.8		± 2.8		± 6.3		± 6.3	
Putamen	16.4	15.9	(-3%)	15.8	(-3.7%)	14.7	(-10.4%)	15.3	(-6.7%)
	± 3.3	± 3.1		± 3.1		± 3.6		± 3.5	
Thalamus	10.3	10	(-2.9%)	9.9	(-3.9%)	9.1	(-11.7%)	9.6	(-6.8%)
	± 2.1	± 2.1		± 2.1		± 2.7		± 2.7	
Cerebellum	6.7	6.6	(-1.5%)	6.5	(-3%)	5.8	(-13.4%)	6.1	(-9%)
	± 1.5	± 1.4		± 1.4		± 2.7		± 2.8	

V_T values are mean ± SD from eight subjects. For Logan and MA1, % differences of V_T relative to two-tissue-compartmental V_T are listed in parentheses.

Supplementary Table 2. Distribution volume (V_T) of [^{11}C]SP203 in human brain analyzed from large regions and individual voxels

	V_T (mL•cm^{-3})							
	Region					Voxel		
Brain regions	Two-comp	Logan $_{VOI}$		MA1$_{VOI}$		Logan $_{Voxel}$		MA1 $_{Voxel}$	
Temporal cortex	26.4	26.7	(1.1%)	26.4	(0%)	22	(-16.7%)	26.9	(1.9%)
	± 2.9	± 3.2		± 3.0		± 3.4		± 3.2	
Cingulate	23.9	24.8	(3.8%)	24.5	(2.5%)	21	(-12.1%)	25.6	(7.1%)
	± 2.1	± 2.2		± 2.1		± 2.3		± 2.2	
Putamen	25	25.2	(0.8%)	25	(0%)	21.6	(-13.6%)	25.3	(1.2%)
	± 3.2	± 3.0		± 3.1		± 3.3		± 3.2	
Thalamus	16.7	17.1	(2.4%)	16.8	(0.6%)	14.4	(-13.8%)	17.4	(4.2%)
	± 2.7	± 2.6		± 2.5		± 2.6		± 2.6	
Cerebellum	9.6	10.2	(6.3%)	10	(4.2%)	7.9	(-17.7%)	10.5	(9.4%)
	± 1.7	± 1.8		± 1.7		± 1.5		± 2.4	

V_T values are mean ± SD from six subjects. For Logan and MA1, % differences of V_T relative to two-tissue-compartmental V_T are listed in parentheses.

Supplementary Table 3. Kinetic rate constants from two-tissue compartment modeling for [^{11}C]FPEB in human brain

Region	K_1 (mL•cm^{-3}•min^{-1})		k_2 (min^{-1})		k_3 (min^{-1})		k_4 (min^{-1})	
Temporal	0.32	(2.7%)	0.27	(14.5%)	0.48	(8.4%)	0.039	(5%)
Cingulate	0.33	(3%)	0.27	(15.3%)	0.44	(9%)	0.041	(5.1%)
Putamen	0.39	(2.2%)	0.24	(10.8%)	0.33	(7.2%)	0.041	(3.5%)
Thalamus	0.36	(1.7%)	0.24	(6%)	0.20	(4.6%)	0.038	(2.1%)
Cerebellum	0.30	(1.1%)	0.17	(3.3%)	0.09	(3.8%)	0.037	(2.3%)

Rate constant values are mean from eight human subjects. For each brain region, mean standard errors for rate constants are listed in parentheses and are expressed as % of the variable itself.

Supplementary Table 4. Kinetic rate constants from two-tissue compartment modeling for [^{11}C]SP203 in human brain

Region	**K_1 (mL•cm^{-3}•min^{-1})**		**k_2 (min^{-1})**		**k_3 (min^{-1})**		**k_4 (min^{-1})**	
Temporal	0.32	(2.5%)	0.20	(12.7%)	0.33	(8.1%)	0.02	(4.5%)
Cingulate	0.32	(3.1%)	0.19	(15.6%)	0.30	(10.3%)	0.02	(5.5%)
Putamen	0.38	(2.2%)	0.14	(10.4%)	0.20	(8%)	0.02	(4%)
Thalamus	0.37	(2%)	0.14	(7.4%)	0.13	(6.6%)	0.02	(3.6%)
Cerebellum	0.29	(1.8%)	0.19	(5%)	0.11	(4.7%)	0.02	(3.2%)

Rate constant values are mean from six human subjects. For each brain region, mean standard errors for rate constants are listed in parentheses and are expressed as % of the variable itself.

Supplementary Table 5. Time-integrated activity coefficient of source organs for [^{11}C]SP203 and [^{11}C]FPEB determined from whole-body imaging of six and eight healthy subjects, respectively.

	Time-integrated activity coefficient (h)					
Organ	**[^{11}C]SP203**			**[^{11}C]FPEB**		
Brain	0.0427	±	0.0088	0.0521	±	0.0083
Gall bladder	0.0150	±	0.0121	0.0163	±	0.0081
Heart wall	0.0035	±	0.0004	0.0020	±	0.0010
Kidneys	0.0117	±	0.0033	0.0080	±	0.0019
Liver	0.0615	±	0.0071	0.0548	±	0.0092
Small intestine	0.0245	±	0.0166	0.0155	±	0.0104
Urinary bladder	0.0224	±	0.0080	0.0179	±	0.0052
Bone marrow	0.0354	±	0.0107	0.0113	±	0.0023
Lungs	0.0096	±	0.0029	-	-	-
Spleen	-	-	-	0.0019	±	0.0014
Thyroid	-	-	-	0.0003	±	0.0001
Remainder in body	0.2639	±	0.0310	0.3101	±	0.0241

Values are mean ± SD.

Supplementary Table 6. Radiation dosimetry estimates for [^{11}C]SP203 and [^{11}C]FPEB determined from six and eight healthy subjects, respectively.

	Radiation dose (μSv/MBq)	
Organ	**[^{11}C]SP203**	**[^{11}C]FPEB**
Adrenals	3.1 ± 0.1	3 ± 0.1
Brain	10.1 ± 2	12.2 ± 2
Breasts	1.7 ± 0.1	1.8 ± 0.1
Gallbladder Wall	38.1 ± 27.7	41.2 ± 20.5
Lower Large Intestine Wall	2.8 ± 0.3	2.7 ± 0.1
Small Intestine	9.8 ± 4.8	7.3 ± 3.2
Stomach Wall	2.5 ± 0.1	2.6 ± 0.1
Upper Large Intestine Wall	3. 5 ± 0.4	3.4 ± 0.2
Heart Wall	4.3 ± 0.4	3 ± 0.9
Kidneys	12 ± 3	8.7 ± 2
Liver	11.5 ± 1.2	10.3 ± 1.7
Lungs	3.6 ± 0.7	2.2 ± 0.1
Muscle	2.1 ± 0.1	2.2 ± 0.1
Ovaries	3 ± 0.4	2.9 ± 0.2
Pancreas	3.1 ± 0.1	3.2 ± 0.2
Red Marrow	5.6 ± 1	3.3 ± 0.2
Osteogenic Cells	5 ± 0.5	3.8 ± 0.2
Skin	1.6 ± 0.1	1.8 ± 0.1
Spleen	2.3 ± 0.1	4 ± 2.3
Testes	1.9 ± 0.2	2.1 ± 0.1
Thymus	2 ± 0.1	2.1 ± 0.1
Thyroid	1.9 ± 0.2	4.1 ± 1.1
Urinary Bladder Wall*	17.1 ± 5.4	14.3 ± 3.8
Uterus	3.3 ± 0.4	3.2 ± 0.2
Total Body	2.8 ± 0	2.8 ± 0
Effective dose	**4.4 ± 0.4**	**3.7 ± 0.2**

* Dynamic urinary bladder model was not used.

Values are expressed as mean ± SD.